Biomolecular Feedback Systems

Domitilla Del Vecchio
MIT

Richard M. Murray
Caltech

Classroom Copy v0.6c, July 11, 2012

Chapter 5
Feedback Examples

In this chapter we present a collection of examples that illustrate some of the modeling and analysis tools covered in the preceding chapters. Each of these examples represents a more complicated system than we have considered previous and together they are intended to demonstrate both the role of feedback in biological systems and how tools from control and dynamical systems can be applied to provide insight and understanding. Each of the sections below is indepedent of the others and they can be read in any order (or skipped entirely).

Pagination in this chapter is broken down by section to faciliate author editing. Review Some extraneous blank pages may be included due to LaTeX processing.

5.1 The *lac* Operon

The *lac* operon is one of the most studied regulatory networks in molecular biology. Its function is to determine when the cell should produce the proteins and enzymes necessary to import and metabolize lactose from its external environment. Since glucose is a more efficient source of carbon, the lactose machinery is not produced unless lactose is present and glucose is not present. The *lac* control system implements this computation.

In this section we construct a model for the lac operon and use that model to understand how changes of behavior can occur for large changes in parameters (e.g., lactose/glucose concentrations) and also the sensitivity of the phenotypic response to changes in individual parameter values in the model. The basic model and much of the analysis in this section is drawn from the work of Yildirim and Mackey [103].

Modeling

In constructing a model for the *lac* system, we need to decide what questions we wish to answer. Here we will attempt to develop a model that allows us to understand what levels of lactose are required for the *lac* system to become active in the absence of glucose. We will focus on the so-called "bistability" of the *lac* operon: there are two steady operating conditions—at low lactose levels the machinery is off and at high lactose levels the machinery is on. The system has hysteresis, so once the operon is actived, it remains active even if the lactose concentration descreases. We will construct a differential equation model of the system, with various simplifying assumptions along the way.

A schematic diagram of the *lac* control system is shown in Figure 5.1. Starting at the bottom of the figure, lactose permease is an integral membrane protein that helps transport lactose into the cell. Once in the cell, lactose is converted to allolactose, and allolactose is then broken down into glucose and galactose, both with the assistance of the enzyme β-galactosidase (β-gal for short). From here, the glucose is processed using the usual glucose metabolic pathway and the galactose.

The control circuitry is implemented via the reactions and transcriptional regulation shown in the top portion of the diagram. The *lac* operon, consisting of the genes *lacZ* (coding for β-gal), *lacY* (coding for lactose permease) and *lacA* (coding for a transacetylase), has a combinatorial promoter. Normally, lac repressor (*lacI*) is present and the operon is off. The activator for the operon is CAP, which has a positive inducer cAMP. The concentration of cAMP is controlled by glucose: when glucose is present, there is very little cAMP available in the cell (and hence CAP is not active).

The bistable switching behavior in the *lac* control system is implemented with a feedback circuit involving the *lac* repressor. Allolactose binds *lac* repressor and so when lactose is being metabolized, then the repressor is sequestered by allolactose

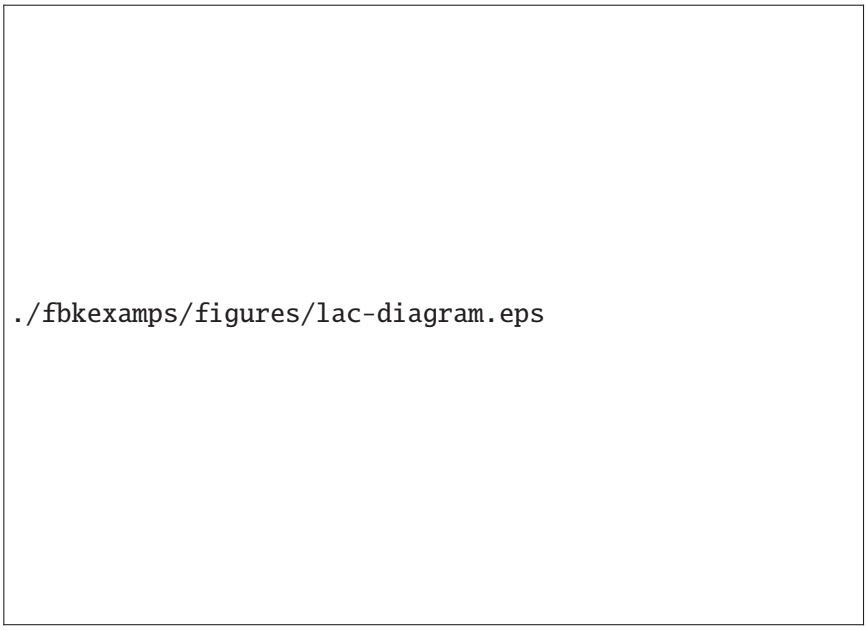

Figure 5.1: Schematic diagram for the *lac* system [103]. Permission pending.

and the *lac* operon is no longer repressed.

To model this circuit, we need to write down the dynamics of all of the reactions and protein production. We will denote the concentration of the β-gal mRNA and protein as m_b and B. We assume that the internal concentration of lactose is given by L, ignoring the dynamics of lactose permease and transport of lactose into the cell. Similarly, we assume that the concentration of repressor protein, denoted R, is constant.

We start by keeping track of the concentration of free allolactose A. The relevant reactions are given by the transport of lactose into the cell, the conversion of lactose into allolactose and then into glucose and lactose and finally the sequestration of repressor R by allolactose:

$$\begin{aligned}
\texttt{Transport:} \quad & \mathrm{L^e + P} \rightleftharpoons \mathrm{L^eP} \longrightarrow \mathrm{L + P} \\
\texttt{Conversion:} \quad & \mathrm{L + B} \rightleftharpoons \mathrm{LB} \longrightarrow \mathrm{A + B} \\
\texttt{Conversion:} \quad & \mathrm{A + B} \rightleftharpoons \mathrm{AB} \longrightarrow \mathrm{Glu + Gal + B} \\
\texttt{Sequestration:} \quad & \mathrm{A + R} \rightleftharpoons \mathrm{AR}
\end{aligned}$$

We see that the dynamics involve a number of enzymatic reactions and hence we can use Michaelis-Menten kinetics to model the response at a slightly reduced level of detail.

Given these reactions, we can write the reaction rate equations to describe the time evolution of the various species concentrations. Let α_X and K_X represent the

parameters of the Michaelis-Menten functions and δ_X represent the dilution and degradation rate for a given species X. The differential equation for the internal lactose concentration L becomes

$$\frac{dL}{dt} = \alpha_{\mathrm{LL^e}} P \frac{L^{\mathrm{e}}}{K_{\mathrm{L^e}} + L^{\mathrm{e}}} - \alpha_{\mathrm{AL}} B \frac{L}{K_{\mathrm{AL}} + L} - \delta_L L, \tag{5.1}$$

where the first term arises from the transport of lactose into the cell, the second term is the conversion of lactose to allolactose, and the final term is due to degradation and dilution. Similarly, the dynamics for the allolactose concentration can be modeled as

$$\frac{dA}{dt} = \alpha_{\mathrm{AL}} B \frac{L}{K_{\mathrm{AL}} + L} - \alpha_{\mathrm{AB}} B \frac{A}{K_A + A} + k^{\mathrm{r}}_{\mathrm{AR}}[\mathrm{AR}] - k^{\mathrm{f}}_{\mathrm{AR}}[\mathrm{A}][\mathrm{R}] - \delta_A A.$$

The dynamics of the production of β-gal and lactose permease are given by the transcription and translational dynamics of protein production. These genes are both part of the same operon (along with *lacA*) and hence the use a single mRNA strand for translation. To determine the production rate of mRNA, we need to determine the amount of repression that is present as a function of the amount of repressor, which in turn depends on the amount of allolactose that is present. We make the simplifying assumption that the sequestration reaction is fast, so that it is in equilibrium and hence

$$[\mathrm{AR}] = k_{\mathrm{AR}}[\mathrm{A}][\mathrm{R}], \qquad k_{\mathrm{AR}} = k^{\mathrm{f}}_{\mathrm{AR}} / k^{\mathrm{r}}_{\mathrm{AR}}.$$

We also assume that the total repressor concentration is constant (production matches degradation and dilution). Letting $R_{\mathrm{tot}} = [\mathrm{R}] + [\mathrm{AR}]$ represent the total repressor concentration, we can write

$$[\mathrm{R}] = R_{\mathrm{tot}} - k_{\mathrm{AR}}[\mathrm{A}][\mathrm{R}] \qquad \Longrightarrow \qquad [\mathrm{R}] = \frac{R_{\mathrm{tot}}}{1 + k_{\mathrm{AR}}[\mathrm{A}]}. \tag{5.2}$$

The simplification that the sequestration reaction is in equilibrium also simplifies the reaction dynamics for allolactose, which becomes

$$\frac{dA}{dt} = \alpha_{\mathrm{AL}} B \frac{L}{K_{\mathrm{AL}} + L} - \alpha_{\mathrm{A}} B \frac{A}{K_A + A} - \delta_A A. \tag{5.3}$$

We next need to compute the effect of the repressor on the production of β-gal and lactose permease. It will be useful to express the promoter state in terms of the allolactose concentration A rather than R, using equation (5.2). We model this using a Hill function of the form

$$F_{\mathrm{BA}}(A) = \frac{\alpha_{\mathrm{R}}}{K_{\mathrm{R}} + R^n} = \frac{\alpha_{\mathrm{R}}(1 + K_{\mathrm{AR}} A)^n}{K_{\mathrm{R}}(1 + K_{\mathrm{AR}} A)^n + R^n_{\mathrm{tot}}}$$

Table 5.1: Parameter values for *lac* dynamics (from [103]).

Parameter	Value	Description
μ	3.03×10^{-2} min^{-1}	dilution rate
α_M	997 nMmin^{-1}	production rate of β-gal mRNA
β_B	1.66×10^{-2} min^{-1}	production rate of β-galactosidase
β_P	??? min^{-1}	production rate of lactose permease
α_A	1.76×10^{4} min^{-1}	production rate of allolactose
γ_M	0.411 min^{-1}	degradation and dilution of β-gal mRNA
δ_B	8.33×10^{-4} min^{-1}	degradation and dilution of β-gal
δ_P	?? min^{-1}	degradation and dilution of lactose permease
δ_A	1.35×10^{-2} min^{-1}	degradation and dilution of allolactose
n	2	Hill coefficient for repressor
K	7200	
k_1	2.52×10^{-2} (μM)$^{-2}$	
K_L	0.97 μM	
K_A	1.95 μM	
β_A	2.15×10^{4} min^{-1}	
τ_M	0.10 min	
τ_B	2.00 min	
τ_P	??? min	

Letting M represent the concentration of the (common) mRNA, the resulting form of the protein production dynamics becomes

$$\begin{aligned}
\frac{dM}{dt} &= e^{-\mu\tau_M} F_{\mathrm{BA}}(A(t-\tau_m)) - \gamma_M M, \\
\frac{dB}{dt} &= \beta_B e^{-\mu\tau_B} M(t-\tau_B) - \delta_B B, \\
\frac{dP}{dt} &= \beta_P e^{-\mu(\tau_M+\tau_P)} M(t-\tau_M-\tau_P) - \delta_P P.
\end{aligned} \tag{5.4}$$

This model includes the degradation and dilution of mRNA (γ_M), the transcriptional delays β-gal mRNA (τ_M), the degradation and dilution of the proteins (δ_B, δ_P) and the delays in the translation and folding of the final proteins (τ_B, τ_P).

To study the dynamics of the circuit, we consider a slightly simplified situation in which we study the response to the internal lactose concentration L. In this case, we can take $L(t)$ as a constant and ignore the dynamics of the permease P. Figure 5.2a shows the time response of the system for an internal lactose concentration of 100 μM. As a test of the effect of time delays, we consider in Figure 5.2b the case when we set the delays τ_M and τ_B to both be zero. We see that the response has very little difference, consistent with our intuition that the delays are short compared to the dynamics of the underlying processes.

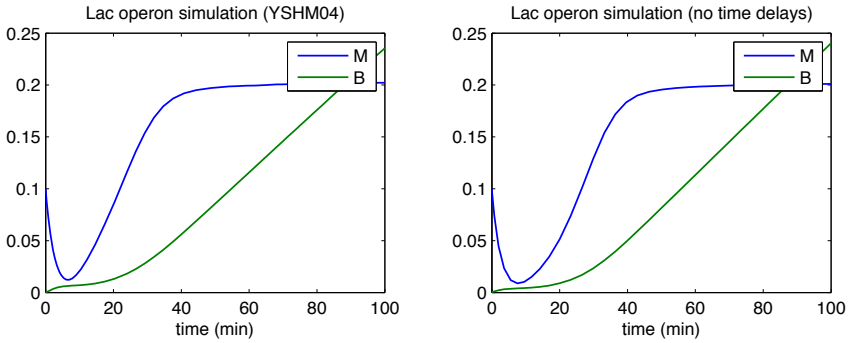

Figure 5.2: Time response of the Lac system.

Bifurcation analysis

To further explore the different types of dynamics that can be exhibited by the Lac system, we make use of bifurcation analysis. If we vary the amount of lactose present in the environent, we expect that the lac circuitry will turn on at some point. Figure 5.3a shows the concentration of allolactose A as a function of the internal lactose concentration L. We see that the behavior of the *lac* system depends on the amount of lactose that is present in the cell. At low concentrations of lactose, the *lac* operon is turned off and the proteins required to metabolize lactose are not expressed. At high concentrations of lactose, the *lac* operon is turned on and the metabolic machinery is activated. In our model, these two operating conditions are measured by the concentration of β-galactosidase B and allolactose A. At intermediate concentrations of lactose, the system has multiple equilibrium points, with two stable equilibrium points corresponding to high and low concentrations of A (and B, as can be verified separately).

The parametric stability plot in Figure 5.3b shows the different types of behavior that can result based on the dilution rate μ and the lactose concentration L. We see that we get bistability only in a certain range of these parameters. Otherwise, we get that the circuitry is either uninduced or induced.

Sensitivity analysis

We now explore how the equilibrium conditions vary if the parameters in our model are changed.

For the gene *lacZ* (which encodes the protein β-galactosidase), we let B represent the protein concentration and M represent the mRNA concentration. We also consider the concentration of the lactose L inside the cell, which we will treat as an external input, and the concentration of allolactose, A. Assuming that the time delays considered previously can be ignored, the dynamics in terms of these variables

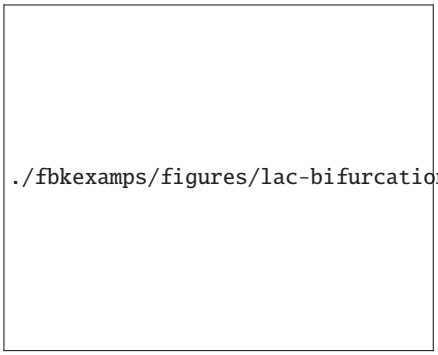

(a) Bifurcation diagram

(b) Stability diagram

Figure 5.3: Bifurcation and stability diagram for the lac system. Figures from [104].

are

$$\begin{aligned}
\frac{dM}{dt} &= F_{BA}(A,\theta) - \gamma_b M, & F_{BA}(A,\theta) &= \alpha_{AB}\frac{1+k_1A^n}{K+k_1A^n},\\
\frac{dB}{dt} &= \beta_B M - \delta_B B, & F_{AL}(L,\theta) &= \alpha_A\frac{L}{k_L+L}, \qquad (5.5)\\
\frac{dA}{ddt} &= BF_{AL}(L,\theta) - BF_{AA}(A,\theta) - \gamma_A A, & F_{AA}(A,\theta) &= \beta_A\frac{A}{k_A+A}.
\end{aligned}$$

Here the state is $x = (M,B,A) \in \mathbb{R}^3$, the input is $w = L \in \mathbb{R}$ and the parameters are $\theta = (\alpha_B,\beta_B,\alpha_A,\gamma_B,\delta_B,\gamma_A,n,k,k_1,k_L,k_A,\beta_A) \in \mathbb{R}^{12}$. The values for the parameters are listed in Table 5.1.

We investigate the dynamics around one of the equilibrium points, corresponding to an intermediate input of $L = 40$ μM. There are three equilibrium points at this value of the input:

$$x_{1,e} = (0.000393, 0.000210, 3.17), \qquad x_{2,e} = (0.00328, 0.00174, 19.4), \qquad x_{3,e} = (0.0142, 0.00758, 42.1).$$

We choose the third equilibrium point, corresponding to the lactose metabolic machinery being activitated and study the sensitivity of the steady state concentrations of allolactose (A) and β-galactosidase (B) to changes in the parameter values.

The dynamics of the system can be represented in the form $dx/dt = f(x,\theta,L)$ with

$$f(x,\theta,L) = \begin{pmatrix} F_{\mathrm{BA}}(A,\theta) - \gamma_B M - \mu M \\ \beta_B M - \delta_B B - \mu B \\ F_{\mathrm{AL}}(L,\theta)B - F_{\mathrm{AA}}(A,\theta)B - \delta_A A - \mu A \end{pmatrix}.$$

To compute the sensitivity with respect to the parameters, we compute the deriva-

tives of f with respect to the state x,

$$\frac{\partial f}{\partial x} = \begin{pmatrix} -\gamma_B - \mu & 0 & \frac{\partial F_{BA}}{\partial A} \\ \beta_B & -\delta_B - \mu & 0 \\ 0 & F_{AL} - F_{\mathrm{AA}} & -B\frac{\partial F_{AA}}{\partial A} \end{pmatrix}$$

and the parameters θ,

$$\frac{\partial f}{\partial \theta} = \begin{pmatrix} F_{BA} & 0 & 0 & -M & 0 & 0 & \frac{\partial F_{BA}}{\partial n} & \frac{\partial F_{BA}}{\partial k} & \frac{\partial F_{BA}}{\partial k_1} & 0 & 0 & 0 \end{pmatrix}.$$

Carrying out the relevant computations and evaluating the resulting expression numerically, we obtain

$$\frac{\partial}{\partial \theta}\begin{pmatrix} B_e \\ A_e \end{pmatrix} = \begin{pmatrix} -1.21 & 0.0243 & -3.35\times 10^{-6} & 0.935 & 1.46 & \dots & 0.00115 \\ -2720. & 47.7 & -0.00656 & 1830. & 2860. & \dots & 3.27 \end{pmatrix}.$$

We can also normalize the sensitivity computation, as described in equation (3.9):

$$S_{x_e\theta} = \frac{\partial x_e / x_e}{\partial \theta / \theta_0} = (D^x)^{-1} S_{x_e\theta} D^\theta,$$

where $D^x = \mathrm{diag}\{x_e\}$ and $D^\theta = \mathrm{diag}\{\theta_0\}$, which yields

$$S_{y_e\theta} = \begin{pmatrix} -4.85 & 3.2 & -3.18 & 3.11 & 3.2 & 6.3 & -6.05 & -4.1 & 4.02 & 6.05 \\ -1.96 & 1.13 & -1.12 & 1.1 & 1.13 & 3.24 & -3.11 & -2.11 & 2.07 & 3.11 \end{pmatrix}$$

where

$$\theta = \begin{pmatrix} \mu & \alpha_M & K & K_1 & \beta_B & \alpha_A & K_L & \beta_A & K_A & L \end{pmatrix}.$$

We see from this computation that increasing the growth rate decreases the equilibrium concentation of B and A, while increasing the lactose concentration by 2-fold increases the equilibrium β-gal concentration 12-fold (6X) and the allolactose concentration by 6-fold (3X).

5.2 Bacterial Chemotaxis

Chemotaxis refers to the process by which micro-organisms move in response to chemical stimuli. Examples of chemotaxis include the ability of organisms to move in the direction of nutrients or move away from toxins in the environment. Chemotaxis is called *positive chemotaxis* if the motion is in the direction of the stimulus and *negative chemotaxis* if the motion is away from the stimulant, as shown in Figure 5.4. Many chemotaxis mechanisms are stochastic in nature, with biased random motions causing the average behavior to be either positive, negative or neutral (in the absence of stimuli).

In this section we look in some detail at bacterial chemotaxis, which *E. coli* use to move in the direction of increasing nutrients. The material in this section is based primarily on the work of Barkai and Leibler [8] and Rao, Kirby and Arkin [81].

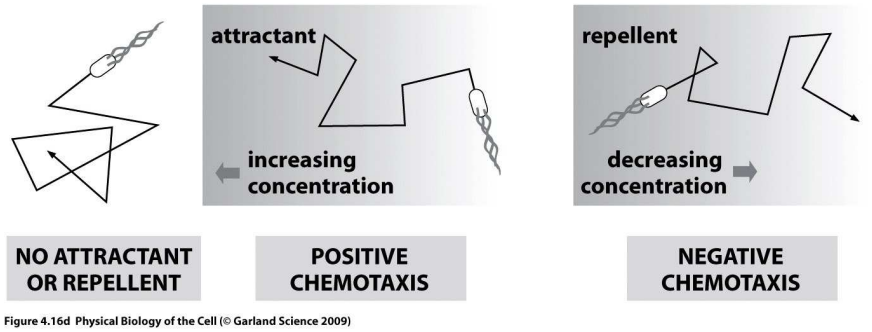

Figure 5.4: Examples of chemotaxis. Figure from Phillips, Kondev and Theriot [76]; used with permission of Garland Science.

Control system overview

The chemotaxis system in *E. coli* consists of a sensing system that detects the presence of nutrients, and actuation system that propels the organism in its environment, and control circuitry that determines how the cell should move in the presence of chemicals that stimulate the sensing system.

The actuation system in the *E. coli* consists of a set of flagella that can be spun using a flagellar motor embedded in the outer membrane of the cell, as shown in Figure 5.5a. When the flagella all spin in the counter clockwise direction, the individual flagella form a bundle and cause the organism to move roughly in a straight line. This behavior is called a "run" motion. Alternatively, if the flagella spin in the clockwise direction, the individual flagella do not form a bundle and the organism "tumbles", causing it to rotate (Figure 5.5b). The selection of the motor direction is controlled by the protein CheY: if phosphorylated CheY binds to the motor complex, the motor spins clockwise (tumble), otherwise it spins counter-clockwise (run).

Because of the size of the organism, it is not possible for a bacterium to sense gradients across its length. Hence, a more sophisticated strategy is used, in which the organism undergoes a combination of run and tumble motions. The basic idea is illustrated in Figure 5.5c: when high concentration of ligand (nutrient) is present, the CheY protein is left unphosphorylated and does not bind to the actuation complex, resulting in a counter-clockwise rotation of the flagellar motor (run). Conversely, if the ligand is not present then the molecular machinery of the cell causes CheY to be phosphorylated and this modifies the flagellar motor dynamics so that a clockwise rotation occurs (tumble). The net effect of this combination of behaviors is that when the organism is traveling through regions of higher nutrient concentration, it continues to move in a straight line for a longer period before tumbling, causing it to move in directions of increasing nutrient concentration.

A simple model for the molecular control system that regulates chemotaxis is

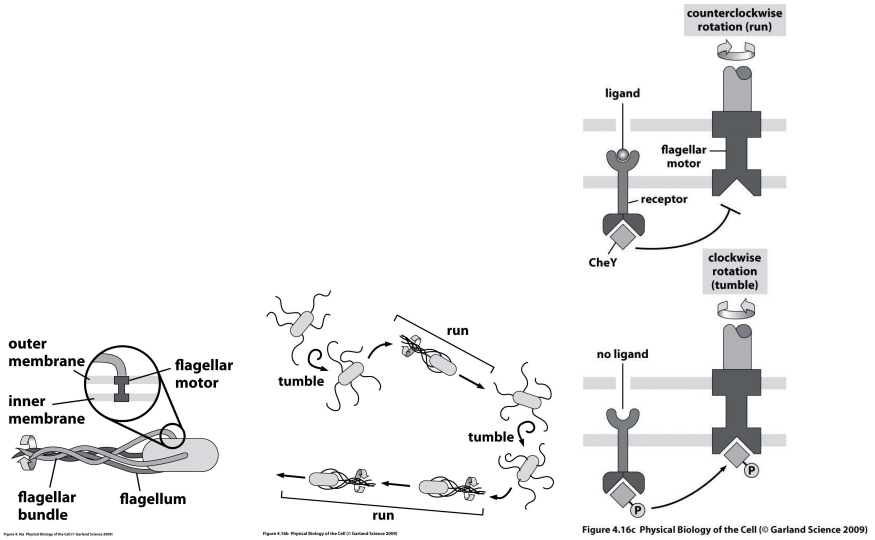

(a) (b) (c)

Figure 5.5: Bacterial chemotaxis. Figures from Phillips, Kondev and Theriot [76]; used with permission of Garland Science.

shown in Figure 5.6. We start with the basic sensing and and actuation mechanisms. A membrane bound protein MCP (methyl-accepting chemotaxis protein) that is capable of binding to the external ligand serves as a signal transducing element from the cell exterior to the cytoplasm. Two other proteins, CheW and CheA, form a complex with MCP. This complex can either be in an active or inactive state. In the active state, CheA is autophosphorylated and serves as a phosphotransferase for two additional proteins, CheB and CheY. The phosphorylated form of CheY then binds to the motor complex, causing clockwise rotation of the motor.

The activity of the receptor complex is governed by two primary factors: the binding of a ligand molecule to the MCP protein and the presence or absence of up to 4 methyl groups on the MCP protein. The specific dependence on each of these factors is somewhat complicated. Roughly speaking, when the ligand L is bound to the receptor then the complex is less likely to be active. Furthermore, as more methyl groups are present, the ligand binding probability increases, allowing the gain of the sensor to be adjusted through methylation. Finally, even in the absence of ligand the receptor complex can be active, with the probability of it being active increasing with increased methylation. Figure 5.7 summarizes the possible states, their free energies and the probability of activity.

Several other elements are contained in the chemotaxis control circuit. The most important of these are implemented by the proteins CheR and CheB, both of which affect the receptor complex. CheR, which is constitutively produced in the cell, methylates the receptor complex at one of the four different methylation sites. Con-

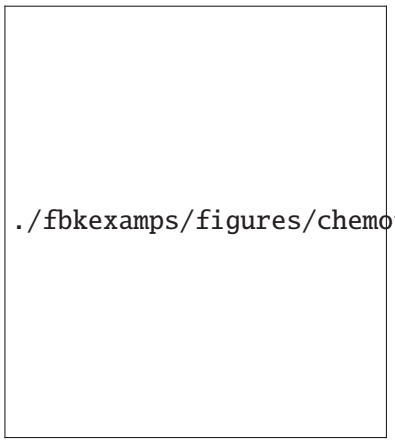

Figure 5.6: Control system for chemotaxis. Figure from Rao *et al*. [81] (Figure 1A).

versely, the phosphorylated form of CheB demethylates the receptor complex. As described above, the methylation patterns of the receptor complex affect its activity, which affects the phosphorylation of CheA and, in turn, phosphorylation of CheY and CheB. The combination of CheA, CheB and the methylation of the receptor complex forms a negative feedback loop: if the receptor is active, then CheA phosphorylates CheB, which in turn demethylates the receptor complex, making it less active. As we shall see when we investigate the detailed dynamics below, this feedback loop corresponds to a type of integral feedback law. This integral action allows the cell to adjust to different levels of ligand concentration, so that the behavior of the system is invariant to the absolute nutrient levels.

Modeling

The detailed reactions that implement chemotaxis are illustrated in Figure 5.8. Letting T represent the receptor complex and T^A represent an active form, the basic reactions can be written as

$$\begin{aligned} T^A + A &\rightleftharpoons T^A{:}A \longrightarrow A^p + T^A \\ A^p + B &\rightleftharpoons A^p{:}B \longrightarrow A + B^p \qquad B^p + P \rightleftharpoons B^p{:}P \longrightarrow B + P \\ A^p + Y &\rightleftharpoons A^p{:}Y \longrightarrow A + Y^p \qquad Y^p + Z \rightleftharpoons Y^p{:}Z \longrightarrow Y + Z \end{aligned} \tag{5.6}$$

where CheA, CheB, CheY and CheZ are written simply as A, B, Y and Z for simplicity and *P* is a non-specific phosphatase. We see that these are basically three linked sets of phosphorylation and dephosphorylation reactions, with CheA serving as a phosphotransferase and P and CheZ serving as phosphatases.

The description of the methylation of the receptor complex is a bit more complicated. Each receptor complex can have multiple methyl groups attached and the

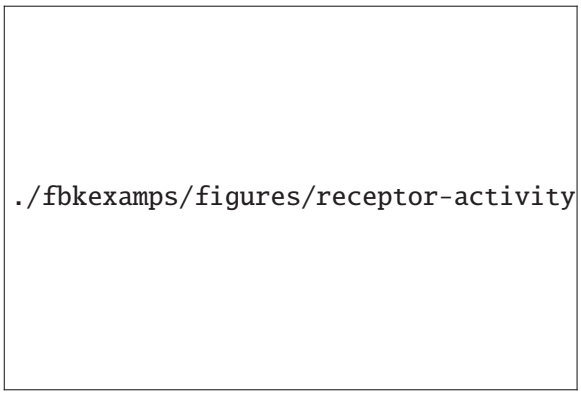

Figure 5.7: Receptor complex states. The probability of a given state being in an active configuration is given by p. Figure obtained from [68].

activity of the receptor complex depends on both the amount of methylation and whether a ligand is attached to the receptor site. Furthermore, the binding probabilities for the receptor also depend on the methylation pattern. To capture this, we use the set of reactions that are illustrated in Figures 5.6 and 5.8. In this diagram, $\mathrm{T}_\mathrm{i}^\mathrm{s}$ represents a receptor that has i methylation sites filled and ligand state s (which can be either u if unoccupied or o if occupied). We let M represent the maximum number of methylation sites ($M = 4$ for *E. coli*).

Using this notation, the transitions between the states correspond to the reactions shown in Figure 5.9:

$$\begin{aligned}
&\mathrm{T}_\mathrm{i}^\mathrm{x} + \mathrm{B}^\mathrm{p} \rightleftharpoons \mathrm{T}_\mathrm{i}^\mathrm{x}{:}\mathrm{B}^\mathrm{p} \longrightarrow \mathrm{T}_{\mathrm{i}-1}^\mathrm{x} + \mathrm{B}^\mathrm{p} && \mathrm{i} > 0,\ x \in \{u, 0\} \\
&\mathrm{T}_\mathrm{i}^\mathrm{x} + \mathrm{R} \rightleftharpoons \mathrm{T}_\mathrm{i}^\mathrm{x}{:}\mathrm{R} \longrightarrow \mathrm{T}_{\mathrm{i}+1}^\mathrm{x} + \mathrm{R} && \mathrm{i} < M,\ x \in \{u, 0\} \\
&\mathrm{T}_\mathrm{i}^\mathrm{u} + \mathrm{L} \rightleftharpoons \mathrm{T}_\mathrm{i}^\mathrm{o}
\end{aligned}$$

We now must write reactions for each of the receptor complexes with CheA. Each form of the receptor complex has a different activity level and so the most complete description is to write a separate reaction for each $\mathrm{T}_\mathrm{i}^\mathrm{o}$ and $\mathrm{T}_\mathrm{i}^\mathrm{u}$ species:

$$\mathrm{T}_\mathrm{i}^\mathrm{x} + \mathrm{A} \underset{k_i^{r,o}}{\overset{k_i^{f,o}}{\rightleftharpoons}} \mathrm{T}_\mathrm{i}^\mathrm{x}{:}\mathrm{A} \xrightarrow{k_i^{c,o}} \mathrm{A}^\mathrm{p} + \mathrm{T}_\mathrm{i}^\mathrm{x},$$

where $\mathrm{x} \in \{\mathrm{o}, \mathrm{u}\}$ and $\mathrm{i} = 0, \ldots, M$. This set of reactions replaces the placeholder reaction $\mathrm{T}^\mathrm{A} + \mathrm{A} \rightleftharpoons \mathrm{T}^\mathrm{A}{:}\mathrm{A} \longrightarrow \mathrm{A}^\mathrm{p} + \mathrm{T}^\mathrm{A}$ used earlier.

Approximate model

The detailed model described above is sufficiently complicated that it can be difficult to analyze. In this section we develop a slightly simpler model that can be

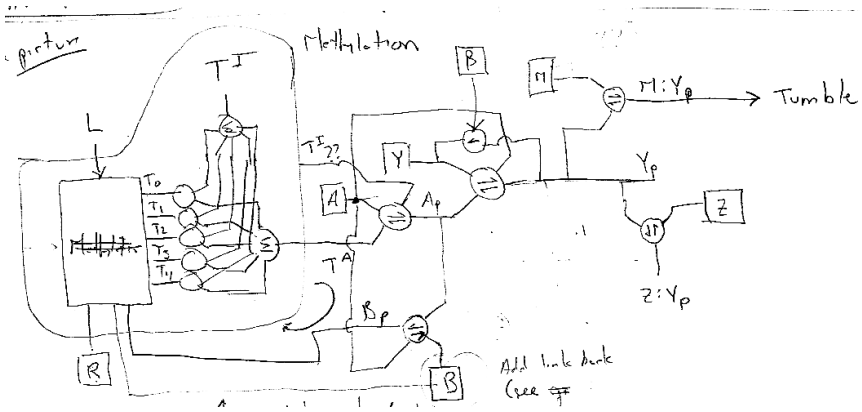

Figure 5.8: Circuit diagram for chemotaxis.

used to explore the adaptation properties of the circuit, which happen on a slower time-scale.

We begin by simplifying the representation of the receptor complex and its methylation pattern. Let $L(t)$ represent the ligand concentration and T_i represent the concentration of the receptor complex with i sides methylated. If we assume that the binding reaction of the ligand L to the complex is fast, we can write the probability that a receptor complex with i sites methylated is in its active state as a static function $\alpha_i(L)$, which we take to be of the form

$$\alpha_i(L) = \frac{\alpha_i^o L}{K_L + L} + \frac{\alpha_i K_L}{K_L + L}.$$

The coefficients α_i^o and α_i capture the effect of presence or absence of the ligand on the activity level of the complex. Note that α_i has the form of a Michaelis-Menten function, reflecting our assumption that ligand binding is fast compared to the rest

./fbkexamps/figures/chemotaxis-methylation.eps

Figure 5.9: Methylation model for chemotaxis. Figure from Barkai and Leibler [8] (Box 1). Note: the figure uses the notation E_i^s for the receptor complex instead of T_i^s.

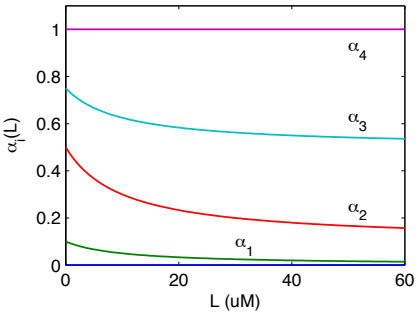

Figure 5.10: Probability of activity.

of the dynamics in the model. Following [81], we take the coefficients to be

$$a_0 = 0, \quad a_1 = 0.1, \quad a_2 = 0.5, \quad a_3 = 0.75, \quad a_4 = 1,$$
$$a_0^o = 0, \quad a_1^o = 0, \quad a_2^o = 0.1, \quad a_3^o = 0.5, \quad a_4^o = 1.$$

and choose $K_L = 10$ μM. Figure 5.10 shows how each α_i varies with L.

The total concentration of active receptors can now be written in terms of the receptor complex concentrations T_i and the activity probabilities $\alpha_i(L)$. We write the concentration of activated complex $\mathrm{T^A}$ and inactivated complex $\mathrm{T^I}$ as

$$T^A = \sum_{i=0}^{4} \alpha_i(L) T_i, \qquad T^I = \sum_{i=0}^{4} (1 - \alpha_i(L)) T_i.$$

These formulas can now be used in our dynamics as an effective concentration of active or inactive receptors, justifying the notation that we used in equation (5.6).

We next model the transition between the methylation patterns on the receptor. We assume that the rate of methylation depends on the activity of the receptor complex, with active receptors less likely to be demethylated and inactive receptors less likely to be methylated [81, 68]. Let

$$r_B = k_B \frac{B^p}{K_B + T^A}, \qquad r_R = k_R \frac{R}{K_R + T^I},$$

represent rates of the methylation and demethylation reactions. We choose the coefficients as

$$k_B = 0.5, \quad K_B = 5.5, \quad k_R = 0.255, \quad K_R = 0.251,$$

We can now write the methylation dynamics as

$$\frac{d}{dt} T_i = r_R(1 - \alpha_{i+1}(L)) T_{i-1} + r_B \alpha_{i+1}(L) T_{i+1} - r_R(1 - \alpha_i(L)) T_i - r_B \alpha_i(L) T_i,$$

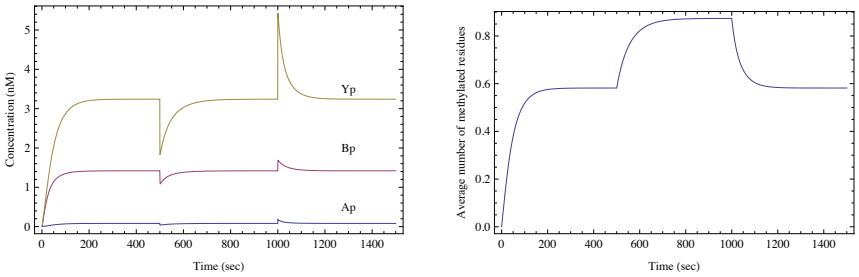

(a) (b)

Figure 5.11: Simulation and analysis of reduced-order chemotaxis model.

where the first and second terms represent transitions into this state via methylation or demethylation of neighboring states (see Figure 5.9) and the last two terms represent transitions out of the current state by methylation and demethylation, respectively. Note that the equations for T_0 and T_4 are slightly different since the demethylation and methylation reactions are not present, respectively.

Finally, we write the dynamics of the phosphorylation and dephosphorylation reactions, and the binding of $\mathrm{CheY^p}$ to the motor complex. Under the assumption that the concentrations of the phosphorylated proteins are small relative to the total protein concentrations, we can approximate the reaction dynamics as

$$\begin{aligned}
\frac{d}{dt}A^p &= 50T^A A - 100A^pY - 30A^pB, \\
\frac{d}{dt}Y^p &= 100A^pY - 0.1Y^p - 5[\mathrm{M}]Y^p + 19[\mathrm{M{:}Y^p}] - 30Y^p, \\
\frac{d}{dt}B^p &= 30A^pB - B^p, \\
\frac{d}{dt}[\mathrm{M{:}Y^p}] &= 5[\mathrm{M}]Y^p - 19[\mathrm{M{:}Y^p}].
\end{aligned}$$

The total concentrations of the species are given by

$$A + A^p = 5\ \mathrm{nM}, \qquad B + B^p = 2\ \mathrm{nM}, \qquad Y + Y^p + [\mathrm{M{:}Y^p}] = 17.9\ \mathrm{nM},$$
$$[\mathrm{M}] + [\mathrm{M{:}Y^p}] = 5.8\ \mathrm{nM}, \qquad R = 0.2\ \mathrm{nM}, \qquad \textstyle\sum_{i=0}^{4} T_i = 5\ \mathrm{nM}.$$

The reaction coefficients and concentrations are taken from Rao *et al*. [81].

Figure 5.11a shows a the concentration of the phosphorylated proteins based on a simulation of the model. Initially, all species are started in their unphosphorylated and demethylated states. At time $T = 500$ s the ligand concentration is increased to $L = 10\ \mu\mathrm{M}$ and at time $T = 1000$ it is returned to zero. We see that immediately after the ligand is added, the $\mathrm{CheY^p}$ concentration drops, allowing longer runs between tumble motions. After a short period, however, the $\mathrm{CheY^p}$ concentration adapts to the higher concentration and the nominal run versus tumble behavior is restored.

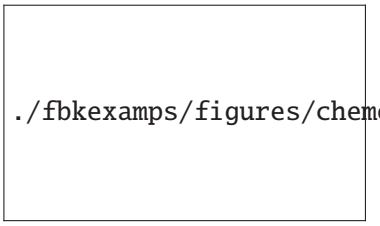

Figure 5.12: Reduced order model of receptor activity. Obtained from [3], Figure 7.9.

Similarly, after the ligand concentration is decreased the concentration of $\mathrm{CheY^p}$ increases, causing a larger fraction of tumbles (and subsequent changes in direction). Again, adaptation over a longer time scale returns that CheY concentration to its nominal value.

Figure 5.11b helps explain the adaptation response. We see that the average amount of methylation of the receptor proteins increases when the ligand concentration is high, which decreases the activity of CheA (and hence decreases the phosphorylation of CheY).

Integral action

The perfect adaptation mechanism in the chemotaxis control circuitry has the same function as the use of integral action in control system design: by including a feedback on the integral of the error, it is possible to provide exact cancellation to constant disturbances. In this section we demonstrate that a simplified version of the dynamics can indeed be regarded as integral action of an appropriate signal. This interpretation was first pointed out by Yi *et al* [102].

We begin by formulating an even simpler model for the system dynamics that captures the basic features required to understand the integral action. Let X represent the receptor complex and assume that it is either methylated or not. We let $\mathrm{X_m}$ represent the methylated state and we further assume that this methylated state can be activated, which we write as $\mathrm{X_m^*}$. This simplified description replaces the multiple states T_i and probabilities $\alpha_i(L)$. We also ignore the additional phosphorylation dynamics of CheY and simply take the activated receptor concentration X_m^* as our measure of overall activity.

Figure 5.12 shows the transitions between the various forms X. As before, CheR methylates the receptor and $\mathrm{CheB^p}$ demethylates it. We simplify the picture by only allowing $\mathrm{CheB^p}$ to act on the active state $\mathrm{X_m^*}$ and CheR to act on the inactive state. We take the ligand into account by assuming that the transition between the active form $\mathrm{X_m^*}$ and the inactive form $\mathrm{X_m}$ depends on the ligand concentration: higher ligand concentration will increase the rate of transition to the inactive state.

This model is a considerable simplification from the ligand binding model that is illustrated in Figures 5.7 and 5.9. In the previous models, there is some prob-

ability of activity with or without methylation and with or without ligand. In this simplified model, we assume that only three states are of interest: demethylated, methylated/inactive and methylated/active. We also modify the way that that ligand binding is captured and instead of keeping track of all of the possibilities in Figure 5.7, we assume that the ligand transitions us from an active state $\mathrm{X_m^*}$ to an inactive $\mathrm{X_m}$. These states and transitions are roughly consistent with the different energy levels and probabilities in Figure 5.7, but it is clearly a much coarser model.

Accepting these approximations, the model illustrated in Figure 5.12 results in a set of chemical reactions of the form

$$\begin{aligned}
&\texttt{R1}: && \mathrm{X + R \rightleftharpoons X{:}R \longrightarrow X_m + R} && \text{methylation}\\
&\texttt{R2}: && \mathrm{X_m^* + B^p \rightleftharpoons X_m^*{:}B^p \longrightarrow X + B^p} && \text{demethylation}\\
&\texttt{R3}: && \mathrm{X_m^* \underset{k^r}{\overset{k^f(L)}{\rightleftharpoons}} X_m} && \text{activation/deactivation}
\end{aligned}$$

For simplicity we take both R and $\mathrm{B^p}$ to have constant concentration.

We can approximate the first and second reactions by their Michaelis-Menten forms, which yield net methylation and demethylation rates (for those reactions)

$$v_+ = k_R R \frac{X}{K_X + X}, \qquad v_- = k_B B^p \frac{X_m^*}{K_{X_m^*} + X_m^*}.$$

If we further assume that $X \gg K_X > 1$, then the methylation rate can be further simplified:

$$v_+ = k_R R \frac{X}{K_X + X} \approx K_R R.$$

Using these approximations, we can write the resulting dynamics for the overall system as

$$\begin{aligned}
\frac{d}{dt} X_m &= k_R R + k^f(L) X_m^* - k^r X_m \\
\frac{d}{dt} X_m^* &= -k_B B^p \frac{X_m^*}{K_{X_m^*} + X_m^*} - k^f(L) X_m^* + k^r X_m.
\end{aligned}$$

We wish to use this model to understand how the steady state activity level X_m^* depends on the ligand concentration L (which enters through the deactivation rate $k^f(L)$).

It will be useful to rewrite the dynamics in terms of the activated complex concentration X_m^* and the *total* methylated complex concentration $X_m^t = X_m + X_m^*$. A simple set of algebraic manipulations yields

$$\begin{aligned}
\frac{dX_m^*}{dt} &= k^r (X_m^t - X_m^*) - k_B B^p \frac{X_m^*}{K_{X_m^*} + X_m^*} - k^f(L) X_m^*, \\
\frac{dX_m^t}{dt} &= k_R R - k_B B^p \frac{X_m^*}{K_{X_m^*} + X_m^*}.
\end{aligned}$$

From the second equation, we see that the the concentration of methylated complex X_m^t is a balance between the action of the methylation reaction (R1, characterized by v_+) and the demethylation reaction (R2, at rate v_-). Since the action of a ligand binding to the receptor complex increases the rate of deactivation of the complex (R3), in the presence of a ligand we will increase the amount of methylated complex (and, via reaction R1) eventually restore the amount of the activated complex. This represents the adaptation mechanism in this simplified model.

To further explore the effect of adaptation, we compute the equilibrium points for the system. Setting the time derivatives to zero, we obtain

$$X_{m,e}^* = \frac{K_{X_m^*} k_R R}{k_B B^p - k_R R}$$
$$X_{m,e}^t = \frac{1}{k^r}\left(k^r X_m^* + k_B B^p \frac{X_m^*}{K_{X_m^*} + X_m^*} + k^f(L) X_m^*\right).$$

Note that the solution for the active complex $X_{m,e}^*$ in the first equation does not depend on $k^f(L)$ (or k^r) and hence the steady state solution is independent of the ligand concentration. Thus, in steady state, the concentration of activated complex adapts to the steady state value of the ligand that is present, making it insensitive to the steady state value of this input.

The dynamics for X_m^t can be viewed as an integral action: when the concentration of X_m^* matches its reference value (with no ligand present), the quantity of methylated complex X_m^t remains constant. But if X_m^t does not match this reference value, then X_m^t increases at a rate proportional to the methylation "error" (measured here by difference in the nominal reaction rates v_+ and v_-). It can be shown that this type of integral action is necessary to achieve perfect adaptation in a robust manner [102].